Macromolecules
ARTICLE

Macromolecules **2010**, *43*, 1061–1068 **1061**
DOI: 10.1021/ma902200z

Conformational, Dimensional, and Hydrodynamic Properties of Amylose Tris(*n*-butylcarbamate) in Tetrahydrofuran, Methanol, and Their Mixtures

Ken Terao,*,† Maiko Murashima,† Yuichi Sano,† Shota Arakawa,† Shinichi Kitamura,‡ and Takashi Norisuye†

†*Department of Macromolecular Science, Osaka University, 1-1 Machikaneyama-cho, Toyonaka, Osaka 560-0043, Japan, and* ‡*Graduate School of Life and Environmental Sciences, Osaka Prefecture University, Gakuen-cho, Nakaku, Sakai, Osaka 599-8531, Japan*

Received October 5, 2009; Revised Manuscript Received October 10, 2009

ABSTRACT: Twelve amylose tris(*n*-butylcarbamate) (ATBC) samples ranging in weight-average molecular weight from 1.7×10^4 to 1.7×10^6 have been prepared and studied by light and small-angle X-ray scattering, sedimentation equilibrium, viscosity, infrared absorption (IR), and optical rotation in methanol (MeOH), tetrahydrofuran (THF), and their mixtures at 25 °C (or 20−25 °C for IR). Data for the mean-square radius of gyration, the particle scattering function, and the intrinsic viscosity are analyzed on the basis of the wormlike chain to yield h (contour length per residue) = 0.32 nm and λ^{-1} (Kuhn's segment length) = 11 nm in MeOH and h = 0.26 nm and λ^{-1} = 75 nm in THF. The high stiffness in THF indicated by λ^{-1} = 75 nm is most likely due to the intramolecular hydrogen bonding (between C=O and NH groups of ATBC) observed as the splitting amide I band in the IR spectra. Furthermore, the h value in this solvent is considerably smaller than the helix pitches per residue of 0.37−0.40 nm for amylose triesters in the crystalline state and those of 0.32−0.42 nm for semiflexible amylose tris(phenylcarbamate) in various solvents (λ^{-1} = 15−24 nm), indicating that the ATBC chain forms a tightly wound helix in THF. As the number of intramolecular hydrogen bonds decreases, i.e., as the MeOH content increases in THF−MeOH mixed solvents, λ^{-1} decreases while h increases. These relationships are successfully explained by a two-state model in which each chain consists of randomly distributed semiflexible (loosely helical) and rodlike (rigid helical) sequences. The resultant h values for the rodlike and semiflexible portions are 0.25−0.26 and 0.32 nm, respectively.

Introduction

Intramolecular hydrogen bonding (H-bonding) may play a decisive role in the conformation of a polymer chain in solution, in that it often stabilizes the secondary structure of biological and synthetic polymers, e.g., α-helices of polypeptides,[1] some foldamers,[2,3] and several synthetic helical polymers.[4,5] Amylose tris(carbamate)s, which have three pairs of N−H and C=O groups capable of forming H-bonds on each pyranose ring, can be classified into such polymers.

Several decades ago, Bittiger and Keilich[6] inferred on the basis of circular dichroism (CD) and optical rotatory dispersion curves in 1,4-dioxane (DIOX) that amylose tris(phenylcarbamate) (ATPC) in solution should assume a helical conformation stabilized by the H-bonds between its N−H and C=O groups. Further, Burchard et al. showed the polymer to be quite stiff in a mixed theta solvent[7] and analyzed its dimensional properties in terms of a few models.[8] In recent work, we detected such intramolecular H-bonds in DIOX and 2-ethoxyethanol (2EE) from the split amide I band in infrared absorption (IR) spectra.[9] The helix pitches (or contour lengths) per residue h (= 0.33 nm) in DIOX and 2EE were slightly shorter than those in esters and a ketone (0.37−0.42 nm).[10] This was a measurable difference in h, but spectroscopic information in the ester and ketone solvents could not be obtained in a relevant range of wavelength. Hence, for the purpose of investigating the relationship between the chain conformation and H-boning, further solution work with ATPC did not seem so inviting.

Amylose tris(*n*-butylcarbamate) (ATBC, Chart 1), which can be used as a chiral stationary phase in gas chromatography,[11] should be suitable for this purpose because of its good solubility in methanol (MeOH) and tetrahydrofuran (THF) allowing infrared absorption measurements around the amide I band. This band sensitively reflects the H-bonding of C=O groups not only of ATPC but also of amylose tris(3,5-dimethylphenylcarbamate) (ADMPC).[12] In this work, we studied conformational, dimensional, and hydrodynamic properties of ATBC in THF, MeOH, and their mixtures by light and small-angle X-ray scattering, viscosity, IR, and optical rotation and found that the polymer assumes a rigid, tight, helical conformation in THF and a relatively flexible, more extended helical conformation in MeOH. When expressed in terms of Kuhn's segment length of the wormlike chain[13] (or more generally the stiffness parameter in the helical wormlike chain[14−16]), the rigidity of the ATBC helix in the former solvent was as high as 75 nm and that in the latter solvent was 11 nm. Analyses of the measured properties leading to these findings are described below, along with the conformation change in THF−MeOH mixtures. It should be noted that few studies have been reported on conformational properties of amylose tris(carbamate)s other than ATPC and ADMPC.[17−19]

Experimental Section

Preparation of ATBC Samples. ATBC samples were synthesized from amylose (eight enzymatically synthesized samples[20])

*Corresponding author. E-mail: kterao@chem.sci.osaka-u.ac.jp.

Published on Web 10/28/2009

and an excess amount of *n*-butylisocyanate in a manner similar to that reported previously for the preparation of ATPC;[9] our method was also substantially the same as that employed by Kubota et al. for amylose tris(cyclohexyl carbamate).[21] The amylose samples ranged in weight-average molecular weight M_w from 6×10^3 to 1×10^6 and had polydispersity indices PDI (ratios of M_w to the number-average molecular weight M_n) less than 1.2. A typical procedure for the ATBC synthesis was as follows.

Pyridine (60 cm^3) and *n*-butyl isocyanate (19 g) were added to an amylose (3.5 g) solution of *N*,*N*′-dimethylacetoamide (33 cm^3, containing 3.0 g LiCl), and the reaction mixture was stirred at 80 °C for 24 h. The solution was then poured into a large amount of water to precipitate ATBC. The product was further purified by successive fractional precipitation with MeOH as a solvent and water as a precipitant to remove LiCl, unreacted *n*-butyl isocyanate, and byproduct. *N*,*N*′-Dimethylacetoamide (dehydrated grade), LiCl, *n*-butyl isocyanate, and MeOH (for the fractionation) were used without further purification, while pyridine was purified by fractional distillation over CaH_2.

Twelve appropriate middle fractions were chosen for the present work. They were reprecipitated from MeOH solutions into water and dried in vacuum at 80 °C for 3 days. The degree of substitution (DS) determined from the mass ratio of carbon to nitrogen by elemental analysis for each sample is presented in Table 1. Its values close to 3 (±0.4) indicate that the three hydroxyl groups on each glucose unit of amylose were fully substituted to *n*-butyl carbamate for any sample. The chemical structure was confirmed by observed chemical shifts of 0.8−1 ppm (methyl protons), 1.2−1.6 ppm (methylene protons), 2.8−5.4 ppm (methylene and pyranose protons), and 6−7.4 ppm (NH protons) in ^1H NMR spectra (JEOL GSX-400) for samples ATBC17K and ATBC130K in $CDCl_3$ at 30 °C and also by absorption bands (in wavenumber) of 3320 cm^{-1} for NH stretching and 1705 cm^{-1} for C=O stretching in IR spectra (JASCO FT/IR8300, the KBr method) for ATBC130K, ATBC260K, ATBC460K, and ATBC900K. The PDI value for each sample was determined by size-exclusion chromatography combined with right and low-angle light scattering and refractive index detectors (SEC-LS), with the result listed in the third column in Table 1.

Chart 1. Chemical Structure of ATBC

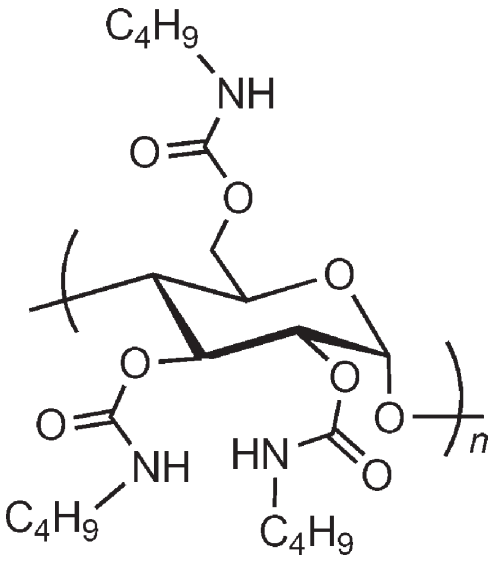

Light and Small-Angle X-ray Scattering. Static light scattering (SLS) measurements were made on a Fica-50 light scattering photometer with vertically polarized incident light of 436 nm wavelength for ATBC1700K, ATBC900K, ATBC700K, ATBC460K, ATBC250K, and ATBC53K in MeOH, for ATBC900K, ATBC700K, ATBC490K, ATBC460K, ATBC260K, and ATBC250K in THF, and for ATBC900K, ATBC700K, and ATBC250K in a THF−MeOH mixture of ϕ_m (the volume fraction of MeOH) = 0.5, all at 25 °C (see ref 9 for the experimental details). The specific refractive index increments $\partial n/\partial c$ for ATBC55K and ATBC17K in MeOH and ATBC900K in THF at 25 °C were determined using a Schulz-Cantow type differential refractometer. The $\partial n/\partial c$ values in MeOH were 0.151, 0.147, and 0.145 $cm^3\ g^{-1}$ at λ_0 (the wavelength) = 436, 546, and 633 nm, respectively, while those in THF were 0.0830, 0.0799, and 0.0795 $cm^3\ g^{-1}$ at 436, 546, and 633 nm, respectively. No substantial difference in $\partial n/\partial c$ between ATBC55K and ATBC17K was observed for MeOH solutions. The THF and MeOH used were fractionally distilled over CaH_2.

Small-angle X-ray scattering (SAXS) experiments were carried out for ATBC55K and ATBC17K in THF−MeOH mixtures with ϕ_m's of 0.25, 0.5, 0.75, and 1 using a Rigaku R-AXIS IV++ or a Rigaku R-AXIS VII imaging plate detector at the BL40B2 beamline in SPring-8. At $\phi_m = 0$, i.e., in pure THF, samples ATBC53K and ATBC17K were studied. The camera length and λ_0 were set to be 1500 mm and 0.1 nm, respectively.

The intensity data obtained from SLS and SAXS were analyzed by use of the square-root plot.[22] The particle scattering function $P(k)$ was evaluated as the ratio of the scattering intensity at zero angle to that at scattering angle θ at infinite dilution, where k denotes the magnitude of the scattering vector.

Sedimentation Equilibrium. Sedimentation equilibrium measurements were made on ATBC17K, ATBC55K, ATBC110K, and ATBC130K in MeOH at 25 °C using a Beckman Optima XL-I analytical ultracentrifuge. Test solutions and the solvent were injected in 12 mm double sector cells and spun at 6500−20 000 rpm. Detailed experimental procedures and data analysis including evaluation of the *z*-average molecular weight M_z were described in ref 23. The partial specific volume was determined to be 0.833 and 0.820 $cm^3\ g^{-1}$ for ATBC17K and

Table 1. Molecular Characteristics of ATBC Samples and Physical Properties in THF and MeOH at 25 °C

			in MeOH				in THF			
sample	DS[d]	PDI	$M_w/10^4$	A_2[e]	$\langle S^2\rangle_z^{1/2}$[f]	$[\eta]$[g]	$M_w/10^4$	A_2[e]	$\langle S^2\rangle_z^{1/2}$[f]	$[\eta]$[g]
ATBC1700K	3.0		167[a]	0.7[a]	53[a]	209				1100
ATBC900K	3.0	1.15[h]	87.0[a]	1.1[a]	38.5[a]	131	90.0[a]	3.2[a]	70[a]	617
ATBC700K	3.0	1.09[h]	67.2[a]	2.3[a]	31[a]	113	73.0[a]	2.6[a]	64[a]	442
ATBC490K	3.0	1.03[h]					49.0[a]	2.8[a]	47[a]	382
ATBC460K	3.0	1.09[h]	45.0[a]	1.4[a]	25.5[a]	100	47.0[a]	2.4[a]	48.5[a]	370
ATBC260K	3.2	1.06[h]					26.3[a]	3.3[a]	33.0[a]	
ATBC250K	2.8	1.07[h]	24.0[a]	1.8[a]	18.5[a]	58.7	25.5[a]	2.7[a]	32.0[a]	180
ATBC130K	3.2	1.02[i]	13.3[c]	1[c]		43.8				100
ATBC110K	3.2	1.05[i]	10.5[c]	1[c]		34.0				70.8
ATBC55K	3.0	1.06[i]	5.45[c]	1[c]	6.6[b]	20.0				31.7
ATBC53K	3.2		5.30[a]	4[a]		21.0			7.7[b]	
ATBC17K	3.4	1.04[i]	1.66[c]	4[c]	2.85[b]	7.1			2.75[b]	8.4

[a] SLS. [b] SAXS. [c] Sedimentation equilibrium. [d] Elemental analysis. [e] In units of 10^{-4} cm^3 mol g^{-2}. [f] In units of nm. [g] In units of $cm^3\ g^{-1}$. [h] M_w/M_n (SEC-LS). [i] M_z/M_w (sedimentation equilibrium).

ATBC55K, respectively, in MeOH at 25 °C using an Anton Paar DMA5000 densitometer. The $\partial n/\partial c$ at $\lambda_0 = 675$ nm was estimated from the above-mentioned data with the aid of $\partial n/\partial c$ vs λ_0^{-2} plot.

Viscometry. The intrinsic viscosity $[\eta]$ at zero shear rate and the Huggins constant k' in THF−MeOH mixtures with different ϕ_m at 25 °C were determined using conventional capillary viscometers and/or a four-bulb low-shear capillary viscometer of the Ubbelohde type. For low-molecular-weight samples, the relative viscosity was evaluated by taking into account the difference between the solution and solvent densities.

Optical Rotation. Specific optical rotations $[\alpha]_{280}$ at λ_0 = 280 nm were determined for ATBC900K, ATBC460K, and ATBC-55K in THF−MeOH mixtures at 25 °C using a JASCO J720WO spectropolarimeter (with an optical rotatory dispersion detector) and a quartz cell of 10 cm path length. The polymer mass concentration c was adjusted to $(1-2) \times 10^{-2}$ g cm^{-3}.

Infrared Absorption and DFT Calculations. Fourier transform infrared absorption (FT-IR) measurements were made for ATBC solutions and the solvents at room temperature (20−25 °C) and at $c \sim 1 \times 10^{-2}$ g cm^{-3} on an Excalibur FTS-300 FT-IR spectrometer (Bio-Rad Laboratories) with a solution cell made of CaF_2 and having 0.05 mm path length.

To assign amide I peaks in experimental IR spectra, calculations based on the density functional theory (DFT) were performed using the Gaussian 03 program.[24] Methyl methylcarbamate (MMC) was chosen as a model compound for the carbonyl groups of ATBC. The absorption wavenumbers ν of amide I and II bands of MMC were found to be 1728 and 1521 cm^{-1}, respectively, when its conformation was optimized using the B3LYP/6-311+G(d,p) level theory with a scaling factor of 0.9679.[25] The absorption bands for an H-bonding carbonyl group were calculated in the following manner. First, an OH group of MeOH or an NH group of an MMC molecule was placed near by the C=O group of another MMC molecule with an appropriate direction. Then the conformation of the complex was optimized by the above-mentioned DFT method. The resultant ν values (amide I) perturbed by MeOH and MMC were obtained as 1704 and 1702 cm^{-1}, respectively.

Results and Discussion

Molecular Weight and Second Virial Coefficient. Figure 1 shows sedimentation equilibrium data for ATBC samples in MeOH (panel a) and SLS data in MeOH (panel b) and in THF (panel c), all at 25 °C. Here, M_{app} is the apparent molecular weight, $\bar{c}$ is the mean concentration defined by $(c_a + c_b)/2$, with c_a and c_b being the polymer mass concentrations at the liquid meniscus and cell bottom, respectively, K is the optical constant, and R_0 is the zero-angle value of the excess reduced scattering intensity R_θ (at scattering angle θ). The values of M_w and A_2 (the second virial coefficient) evaluated from the intercepts and slopes of the indicated straight lines are summarized in Table 1, along with those of M_z/M_w from sedimentation equilibrium. The M_w values in MeOH and THF (for ATBC900K, ATBC700K, ATBC-460K, and ATBC250K) agree with each other within experimental errors (±4%). The A_2 values ranging from 0.7×10^{-4} to 4×10^{-4} cm^3 mol g^{-2} in the two solvents indicate that both are good solvents for ATBC. While A_2 (and M_w) in the mixed solvent was not determined owing to the difficulty to obtain its refractive index increments $(\partial n/\partial c)_\mu$ at fixed chemical potentials μ of diffusible components, THF−MeOH mixtures should also be good solvents because no turbidity were found in the range of temperature between 0 and 40 °C.

Figure 2 illustrates the angular dependence of $P(k)^{-1/2}$ for the indicated ATBC samples in MeOH and THF. The

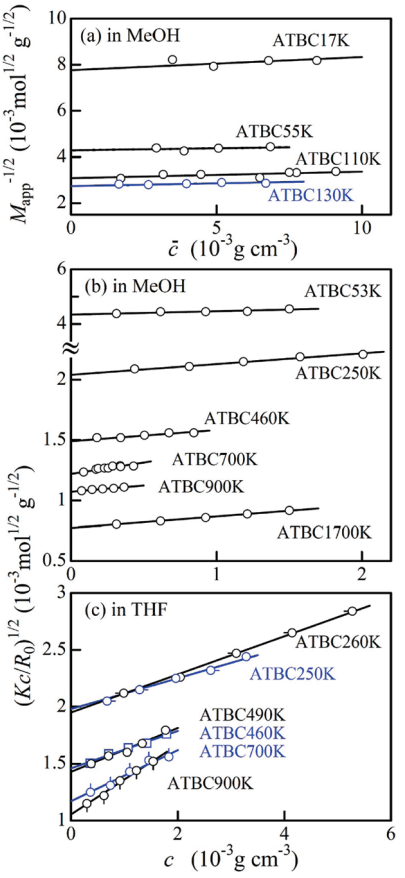

Figure 1. Plots of $M_{app}^{-1/2}$ vs $\bar{c}$ for indicated ATBC samples in MeOH at 25 °C (a) and those of $(Kc/R_0)^{1/2}$ vs c in MeOH (b) and THF (c) at 25 °C.

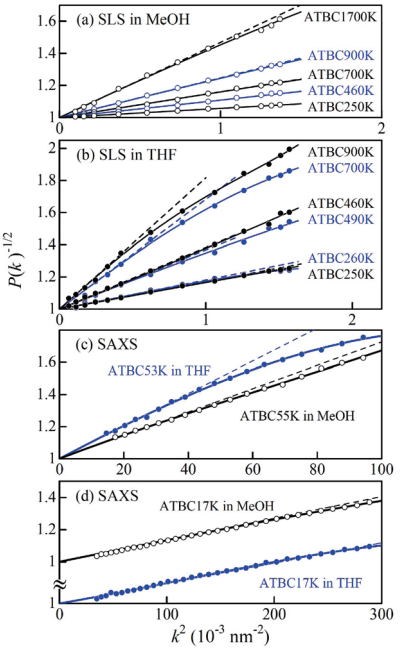

Figure 2. Berry plots for indicated ATBC samples in THF (filled circles) and in MeOH (open circles) at 25 °C: (a) SLS in MeOH, (b) SLS in THF, and (c, d) SAXS.

z-average mean-square radii of gyration $\langle S^2 \rangle_z$ determined from the initial slopes (the dashed lines) of the curves are presented in Table 1, in which $[\eta]$ data are also presented.

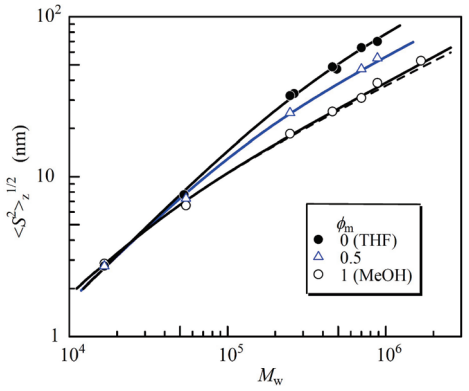

Figure 3. Molecular weight dependence of $\langle S^2 \rangle_z^{1/2}$ for ATBC in THF (filled circles), MeOH (open circles), and a THF−MeOH mixture of $\phi_m = 0.5$ (triangles) at 25 °C. Solid curves: theoretical values calculated for the wormlike chains with the parameters in Table 2. The dashed curve shows the theoretical values for $B = 0$.

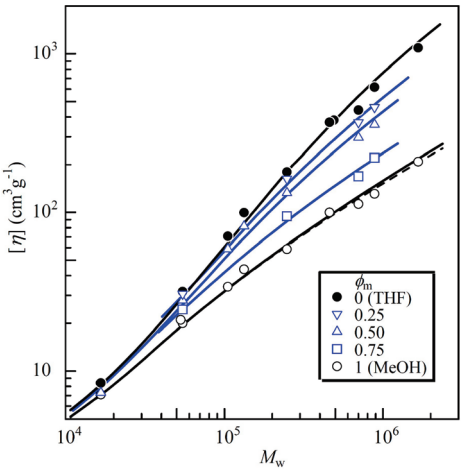

Figure 4. Molecular weight dependence of $[\eta]$ for ATBC in THF (filled circles), MeOH (open circles), and their mixtures (inverted triangles, $\phi_m = 0.25$; triangles, $\phi_m = 0.5$; squares, $\phi_m = 0.75$) at 25 °C. Solid curves: theoretical values calculated for the wormlike chains with the parameters in Table 2. The dashed curve shows the theoretical values for $B = 0$.

Dimensional and Hydrodynamic Properties. *Molecular Weight Dependence of* $\langle S^2 \rangle_z$ *and* $[\eta]$. Figure 3 illustrates the molecular weight dependence of $\langle S^2 \rangle_z^{1/2}$ for ATBC in THF and MeOH at 25 °C. The data points in either solvent are fitted by a curve convex upward, whose slope decreases with increasing M_w from 0.9 to 0.7 and 0.7 to 0.55 in THF and MeOH, respectively, indicating that the ATBC chain is significantly stiffer in the former solvent than in the latter. The figure includes the $\langle S^2 \rangle_z^{1/2}$ data in the THF−MeOH mixture of $\phi_m = 0.5$. The curve fitting the triangles suggests that the polymer in this mixture has a stiffness intermediate between those in THF and MeOH.

The intrinsic viscosities in THF, MeOH, and their mixtures of $\phi_m = 0.25$, 0.50, and 0.75 are plotted double-logarithmically against M_w in Figure 4. The viscosity exponent is 1.2 around $M_w = 10^5$ in THF and decreases with increasing ϕ_m to 0.85 in MeOH, being consistent with the higher stiffness of the ATBC chain in the former solvent found above from $\langle S^2 \rangle_z$.

Analysis of $\langle S^2 \rangle_z$. We analyze the present $\langle S^2 \rangle_z$ data in terms of the wormlike chain with or without excluded volume using the expression[26]

$$\langle S^2 \rangle_0 = \frac{L}{6\lambda} - \frac{1}{4\lambda^2} + \frac{1}{4\lambda^3 L} - \frac{1}{8\lambda^4 L^2}[1 - \exp(-2\lambda L)] \quad (1)$$

for the unperturbed mean-square radius of gyration $\langle S^2 \rangle_0$ and the Domb−Barrett[27] equation for the expansion factors α_S^2 ($= \langle S^2 \rangle / \langle S^2 \rangle_0$) in the quasi-two-parameter (QTP) theory.[14,28,29] Here, λ^{-1} is the Kuhn segment length and L is the contour length equal to the ratio of M (the molar mass) to M_L (the molar mass per unit contour length). In the QTP scheme, $\langle S^2 \rangle$ is a function of M/M_L, λ^{-1}, and B (the excluded-volume strength). The three unknowns (M_L, λ^{-1}, and B) were determined by curve fitting, with the result summarized in Table 2; the values of B in THF and in the mixture of $\phi_m = 0.5$ need not be estimated because excluded-volume effects were negligible in the range of M_w studied. The solid lines fitting the data points in Figure 3 represent the theoretical values, while the dashed line (drawn for MeOH solutions) refers to the unperturbed state. The deviation of the solid line for MeOH from the dashed one is only about 6% at the highest M_w, showing that the intramolecular excluded-volume effect in the solvent is insignificant in the molecular weight range studied.

Analysis of $P(k)$. The Holtzer plots[30] of $k\,P(k)$ vs k for ATBC53K and ATBC17K in THF are shown in Figure 5, along with those for ATBC55K and ATBC17K in MeOH and THF−MeOH mixtures. The data points in THF are quantitatively reproduced by the solid lines computed from Nakamura and Norisuye's theory[31] for wormlike cylinders with $M_L = 1780\ \text{nm}^{-1}$, $\lambda^{-1} = 78$ nm (the value from $\langle S^2 \rangle_z$), and $d = 1.1$ nm. These lines are almost indistinguishable from the dashed curves (mostly hidden behind the solid lines) calculated for the straight cylinders[31,32] with $M_L = 1780\ \text{nm}^{-1}$ and the diameter $d = 1.1$ nm. Thus, the scattering functions of the low-M_w samples do not allow λ^{-1} to be estimated.

In MeOH, a broad but clear peak is observed for ATBC55K (Figure 5), indicating a lower chain stiffness in the solvent than in THF. By curve fitting, M_L, λ^{-1}, and d in this solvent have been estimated on the basis of the theory[31] for unperturbed wormlike cylinders to be $1450 \pm 30\ \text{nm}^{-1}$, 9 ± 2 nm, and 1.1 ± 0.1 nm, respectively. The theoretical solid curves calculated for ATBC55K and ATBC17K with these parameters are appreciably higher than the dashed curves drawn for $\lambda^{-1} = \infty$, thus showing unequivocal determination of λ^{-1} in MeOH. In the mixtures of $\phi_m = 0.25$, 0.5, and 0.75, the $P(k)$ data were similarly analyzed; at $\phi_m = 0.5$ and 0.25, the λ^{-1} values from $\langle S^2 \rangle_z$ and $[\eta]$ (see below), respectively, were assumed. The model parameters obtained from $P(k)$ are presented in Table 2. It should be noted in relation to the d values that the chain thickness contribution[33] $d^2/8$ to $\langle S^2 \rangle$ of a wormlike cylinder is at most 2% and hence negligible in the M_w range studied.

Analysis of $[\eta]$. If the Yamakawa−Fujii−Yoshizaki viscosity theory[14,34,35] for unperturbed wormlike cylinders is combined with the Barrett equation[36] for the viscosity expansion factor in the QTP scheme,[14] $[\eta]$ for a given M is determined by the four parameters: M_L, λ^{-1}, d, and B. In our curve-fitting procedure, the last parameter was considered only in pure MeOH, but M_L in it was taken to be $1440\ \text{nm}^{-1}$, the mean from $\langle S^2 \rangle_z$ and $P(k)$; furthermore, at $\phi_m = 0.25$ and 0.75, the values from $P(k)$ were assumed. The estimated parameters are summarized in Table 2, and the theoretical curves are shown in Figure 4. The dashed line again refers to the unperturbed state.

In Table 2, the values of M_L and λ^{-1} from $[\eta]$ are seen to be in substantial agreement with those from $\langle S^2 \rangle_z$ and $P(k)$, demonstrating that the wormlike chain allows a consistent description of the measured dimensional and hydrodynamic

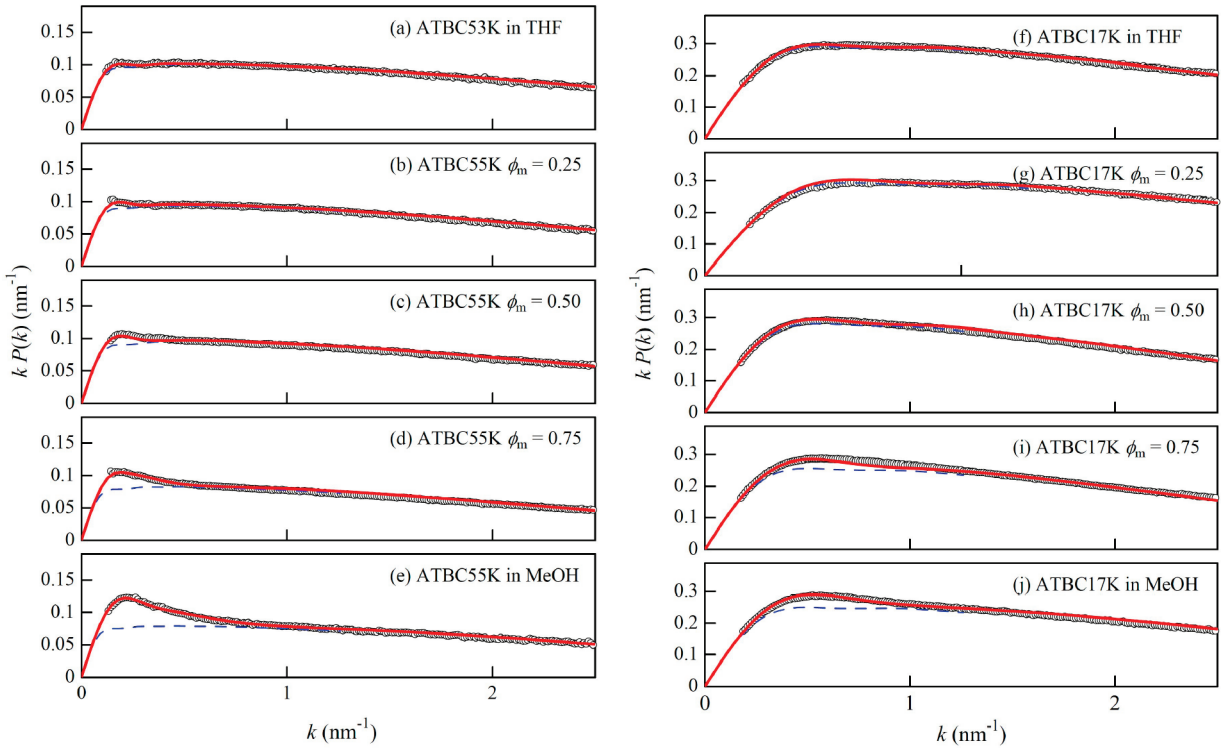

Figure 5. Holtzer plots for ATBC samples in THF, MeOH, and their mixtures at 25 °C. Solid curves: theoretical values for the unperturbed wormlike cylinders with the parameters in Table 2. Dashed curves: theoretical values in the rod limit ($\lambda^{-1} = \infty$).

Table 2. Wormlike Chain Parameters for ATBC in THF, MeOH, and Their Mixtures at 25 °C

method	M_L (nm^{-1})	λ^{-1} (nm)	d (nm)	B (nm)
		in THF		
$\langle S^2\rangle_z$	1750 ± 50	78 ± 4		
$P(k)$	1780 ± 30	78[a]	1.1 ± 0.1	
$[\eta]$	1730 ± 80	70 ± 10	2.7 ± 0.4	
		in MeOH		
$\langle S^2\rangle_z$	1430 ± 100	12 ± 3		0.5 ± 0.5
$P(k)$	1450 ± 30	9 ± 2	1.1 ± 0.1	
$[\eta]$	1440[a]	11 ± 1	2.2 ± 0.1	0.2 ± 0.2
		in the THF−MeOH mixture of ϕ_m = 0.5		
$\langle S^2\rangle_z$	1700 ± 50	35 ± 3		
$P(k)$	1730 ± 30	35[a]	1.3 ± 0.2	
$[\eta]$	1650 ± 70	35 ± 7	2.5 ± 0.3	
		in the THF−MeOH mixture of ϕ_m = 0.25		
$P(k)$	1750 ± 30	45[a]	1.2 ± 0.1	
$[\eta]$	1750[a]	45 ± 3	3.3 ± 0.5	
		in the THF−MeOH mixture of ϕ_m = 0.75		
$P(k)$	1530 ± 30	16 ± 3	1.3 ± 0.1	
$[\eta]$	1530[a]	17 ± 1	2.7 ± 0.5	

[a] Assumed.

properties of ATBC. The d values from $[\eta]$ are, however, 2−3 times larger than those from $P(k)$. This is probably because the latter reflects the electron density profile around the chain contour.[14] Similar behavior was also reported for ATPC[9,10] and other polymers[37,38] in dilute solution.

Wormlike Chain Parameters. Table 3 presents the value of λ^{-1} (the mean from the three different properties) and the contour length per residue h ($= M_0/M_L$) as a function of ϕ_m, where M_0 denotes the molar mass of the repeating unit of

Table 3. Values of h and λ^{-1} for ATBC in THF−MeOH Mixtures at 25 °C

ϕ_m	h (nm)	λ^{-1} (nm)
0 (THF)	0.26 ± 0.01	75 ± 5
0.25	0.26 ± 0.01	45 ± 3
0.5	0.27 ± 0.01	35 ± 3
0.75	0.30 ± 0.01	17 ± 2
1 (MeOH)	0.32 ± 0.01	11 ± 2

ATBC. As ϕ_m decreases, h slightly decreases, while λ^{-1} increases significantly and reaches a value as high as 75 nm in THF. No such high stiffness has ever been reported for other carbamate derivatives of polysaccharides including cellulose,[39−41] chitosan,[42] and mannan.[43] It is interesting to note that amylose has a much smaller λ^{-1} of 4 nm in various solvents[44,45] and a relatively large value of 18 nm in a metal complex solvent.[46] The high rigidity of the ATBC chain in THF is supported by our finding[47] that a concentrated THF solution of the polymer (c = 0.35 g cm^{-3}) shows liquid crystallinity. On the other hand, the h value 0.26 nm in THF, measurably smaller than 0.32 nm in MeOH and 0.33 nm for locally helical ATPC in DIOX and 2EE,[9] is much smaller than those of 0.37−0.42 nm for ATPC in ester and ketone solvents[10] and the helix pitches per residue (0.37−0.40 nm) of amylose triesters in the crystalline state.[48,49] Hence, ATBC in THF may be considered to have a rigid, tight, helical structure; note that the helical wormlike chain model is not necessary for use in analyzing our solution data because the centroid of a helical, stiff polymer chain is represented by the wormlike chain.[50]

Infrared Absorption and Optical Rotation. If a certain local conformation change causes the observed decrease in h and increase in λ^{-1} with a decrease in ϕ_m, it should be detected as changes in IR spectrum and/or optical rotation. Figure 6 displays IR spectra for ATBC460K in THF, MeOH, and their mixtures. While the peaks observed between 1100 and

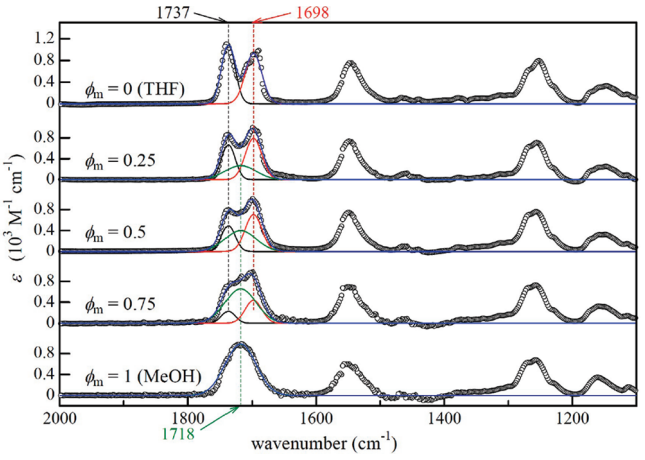

Figure 6. IR spectra (molar absorption coefficient ε vs wavenumber) for ATBC460K in mixtures of THF and MeOH with indicated ϕ_m at room temperature (20−25 °C).

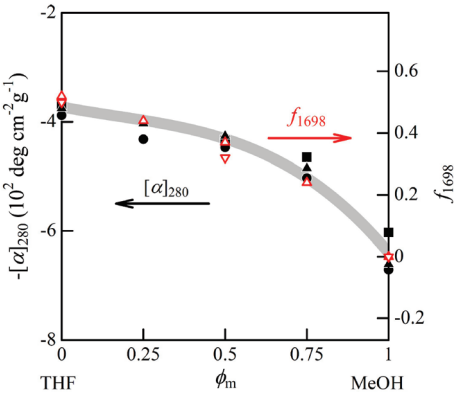

Figure 7. ϕ_m dependence of $-[\alpha]_{280}$ (filled symbols) and f_{1698} (open symbols) for ATBC900K (circles), ATBC460K (triangles), ATBC55K (squares), and ATBC17K (inverted triangles).

1600 cm^{-1} are essentially independent of ϕ_m, the absorption band around 1700−1740 cm^{-1} significantly varies with ϕ_m. The double peak observed in THF is fitted by two Gaussian distributions centered at 1737 and 1698 cm^{-1}. These are fairly close to the theoretical values of 1728 and 1702 cm^{-1} for free and H-bonding carbonyl groups of MMC, respectively (see Experimental Section). On the other hand, the observed single peak in MeOH follows the normal distribution with the mean value of 1718 cm^{-1}, which is larger than the theoretical value 1704 cm^{-1}. This discrepancy and the broad distribution are most likely due to the high mobility of the H-bonding solvent molecules.

IR spectra at the amide I band in THF−MeOH mixtures were successfully separated into the aforementioned three components, as indicated by thin lines in Figure 6. Since the total areas of this band at the five ϕ_m's are substantially the same, we regard the absorption coefficients for the three peaks as equal and denote the area fractions (i.e., the number fractions of the respective components) as f_{1737}, f_{1718}, and f_{1698} at 1737, 1718, and 1698 cm^{-1}, respectively. Both f_{1737} and f_{1698} decrease (and hence f_{1718} increases) with an increase in ϕ_m, and the more abrupt diminution of the former than the latter suggests that the free C=O has higher tendency to form H-bonds with MeOH than does the H-bonding C=O.

Figure 7 illustrates the ϕ_m dependence of f_{1698} and $-[\alpha]_{280}$. The curves of f_{1698} and $-[\alpha]_{280}$ almost overlap each other, indicating that f_{1698} reflects a local-conformational property such as the helix content. The figure also shows that f_{1698} and

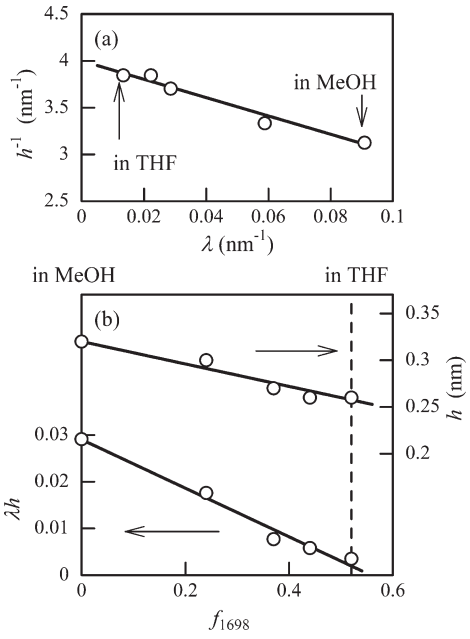

Figure 8. Plots of (a) h^{-1} vs λ and (b) h and λh vs f_{1698} for ATBC in mixtures of THF and MeOH.

$[\alpha]_{280}$ are independent of M_w and undergo monotonic and gradual solvent dependence. Thus, the cooperativity of the helical conformation is much less important for ATBC than for α-helical polypeptides[51,52] or even negligible. In other words, intramolecular H-bonds randomly break as ϕ_m increases, and thus the ATBC chain consists of alternating rigid (helical) and semiflexible (looser helical) portions with and without intramolecular H-bonding, respectively.

Solvent Dependence of Main Chain Conformation. On the basis of the above considerations, we model the ATBC chain in a given THF−MeOH mixture by a copolymer consisting of R and F monomeric units and denote the Kuhn lengths of the pure R and F chains as λ_R^{-1} and λ_F^{-1}, respectively, and the contour lengths per residue as h_R and h_F. We assume the distribution of these units to be completely random. Then h ($= M_0L/M$) and λ^{-1} leading to eq 1 are given by[53]

$$h = F_R h_R + (1 - F_R) h_F \tag{2}$$

$$\lambda h = F_R \lambda_R h_R + (1 - F_R) \lambda_F h_F \tag{3}$$

where the number fraction F_R of the R monomer is related to f_{1698} by

$$F_R = \frac{f_{1698}}{f_R} \tag{4}$$

with f_R the value of f_{1698} for the homopolymer R; note that f_F (f_{1698} for the F homopolymer) = 0 because f_{1698} vanishes in MeOH. Elimination of F_R from eqs 2 and 3 yields

$$h^{-1} - h_F^{-1} = -\frac{h_R^{-1} - h_F^{-1}}{\lambda_F - \lambda_R}(\lambda - \lambda_F) \tag{5}$$

which predicts that h^{-1} varies linearly with λ.

Panel a of Figure 8 shows the plot of h^{-1} vs λ constructed for ATBC in THF−MeOH mixtures according to eq 5, while panel b presents those of h and λh against f_{1698} based on eqs 2 and 3, respectively. These plots are linear, implying that the two-state model assumed is suitable for describing the

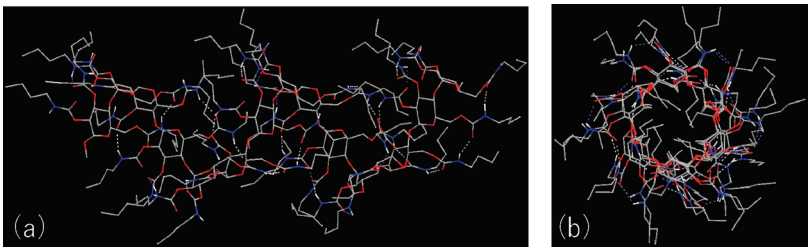

Figure 9. A possible 3D structure of rigid helical ATBC (6-fold helix and h = 0.25 nm): (a) side view; (b) top view.

conformation change of ATBC in the mixed solvent system. The intercepts of the straight lines in panel b give $h_F = 0.32$ nm and $\lambda_F^{-1} = 11$ nm (see also Table 3). With these values for the F polymer, we obtain the relation $h_R^{-1} = 4.0 - 9.8\lambda_R$ (nm^{-1}) for the R polymer using eq 5 and the slope (−9.8) of the line in panel a. Although any single relation does not allow determination of two unknowns, we can estimate h_R to be in a narrow range between 0.25 and 0.26 nm on the basis of the possible λ_R range ($0 < \lambda_R < 1/75$ nm^{-1}); note that the contribution of $-9.8\lambda_R$ in the above relation to h_R is at most 3.3%. The h_R of 2.5−2.6 nm does not differ from the directly estimated value of 0.26 nm in THF, both being much shorter than 0.37−0.42 nm for ATPC in ester and ketone solvents[8] and for amylose triesters in the crystalline state.[48,49] Using the h vs f_{1698} relation (the upper straight line in panel b) with h_R = 0.25−0.26 nm, we estimate f_R ($> f_{1698}$ in THF) to be 0.52−0.58. The f_R in this range is fairly close to the value 2/3 corresponding to the case in which two C=O groups per repeating unit of the R chain form H-bonds (i.e., $f_R = 2/3$).

We add that the copolymer nature mentioned above does not impair the wormlike chain behavior of $[\eta]$ and $P(k)$ if the diameters of the R and F chains are not very different. In fact, the wormlike chain parameters (M_L and λ^{-1}) determined from the different methods are in excellent agreement with one another for ATBC in the mixed solvent of $\phi_m = 0.5$ and for an actual copolymer.[53] This is also supported by the theoretical fact that the conformational defect in the broken wormlike chain model has no significant effect on dimensional and hydrodynamic properties.[54]

Possible Helical Structure. To determine the helical structure of an amylosic chain, at least two torsion angles should be given even when the glucosidic bond angle and the conformation of the pyranose ring are fixed, but we have only one piece of information, that is, h. We note that the 2D NOESY NMR method reported to estimate the distance between two hydrogen atoms on consecutive pyranose rings of ADMPC[17] is not applicable to our system since the signal of some methylene protons of ATBC is hardly distinguishable from that of some pyranose protons. Therefore, we can deduce the helical structure of ATBC on condition that the helical symmetry is available.

We chose a 6-fold left-handed helix of h = 0.25 nm and attempted to construct the structure of a 14-mer ATBC molecule using the sugar builder of the Hyperchem version 8 software. An MM2 minimization was performed on the molecule using the ChemBioOffice Ultra 11.0 (some parameters were guessed by the algorithm of the software) after the molecular dynamics simulation with the same force field for 20 ps (10 000 steps) at 300 K. In these procedures, oxygen atoms between every two consecutive pyranose rings were fixed to keep the h value. The resultant 3D structure displayed in Figure 9 shows that most of the C=O groups at C2 and C6 of the respective pyranose rings form H-bonds with the NH groups at C3 and C6 on the next adjoining pyranose rings, respectively (the white dotted segments), whereas each C=O at C3 has no or a weak H-bond with the NH group on the same repeat unit. Namely, the number fraction of strongly H-bonding C=O groups is roughly 0.6, a value fairly close to experimentally estimated f_R of 0.52−0.58. The agreement suggests that the displayed 3D conformation is one of the possible helical structures for ATBC in THF. We note, however, that this discussion also applies to 5- or 7-fold helices. It is thus intriguing to determine the crystal structure of the amylose derivative, but we wish to leave the determination for future work.

Conclusions

ATBC in THF assumes a rigid helical conformation with λ^{-1} = 75 nm and h = 0.26 nm stabilized by intramolecular H-bonds. This helix pitch per residue is much shorter than the reported values for ATPC in ketone and ester solvents (0.37−0.42 nm)[10] and for amylose triesters in the crystalline state (0.37−0.40 nm).[48,49] On the other hand, the ATBC helix in MeOH is much more flexible (λ^{-1} = 11 nm) and slightly extended (h = 0.32 nm), as is the case for the ATPC helices in DIOX and 2EE.[9] In mixtures of THF and MeOH, λ^{-1}, h, the number fraction f_{1698} of the intramolecular H-bonding, and $[\alpha]_{280}$ change monotonically with MeOH content. The last two quantities, independent of M_w, indicate that the cooperativity does not play an important role in the solvent-induced conformation change for the polymer−mixed solvent system. This conformation change is successfully explained by a two-state model consisting of random sequences of rodlike and semiflexible portions, i.e., by random breaking of intramolecular hydrogen bonds in ATBC accompanying an increase in MeOH content.

Acknowledgment. We are indebted to Prof. Takahiro Sato (Osaka Univ.) for valuable discussions and comments, Prof. Tadashi Inoue (Osaka Univ.) for allowing us to use the FT-IR instrument, and Mr. Masahiro Ohtoh (Osaka Univ.) for synthesis of an ATBC sample. The synchrotron radiation experiments were performed at the BL40B2 in SPring-8 with the approval of the Japan Synchrotron Radiation Research Institute (JASRI) (Proposal #2007A1034 and #2007B1296).

References and Notes

(1) Alberts, B.; Johnson, A.; Lewis, J.; Raff, M.; Roberts, K.; Walter, P. *Molecular Biology of the Cell*, 4th ed.; Garland Science: New York, 2002.
(2) Gellman, S. H. *Acc. Chem. Res.* **1998**, *31*, 173–180.
(3) Hill, D. J.; Mio, M. J.; Prince, R. B.; Hughes, T. S.; Moore, J. S. *Chem. Rev.* **2001**, *101*, 3893–4011.
(4) Okoshi, K.; Sakurai, S.-I.; Ohsawa, S.; Kumaki, J.; Yashima, E. *Angew. Chem., Int. Ed.* **2006**, *45*, 8173–8176.
(5) Terada, K.; Masuda, T.; Sanda, F. *Macromolecules* **2009**, *42*, 913–920.
(6) Bittiger, H.; Keilich, G. *Biopolymers* **1969**, *7*, 539–556.
(7) Burchard, W. *Br. Polym. J.* **1971**, *3*, 214–221.
(8) Hsu, B.; McWherter, C. A.; Brant, D. A.; Burchard, W. *Macromolecules* **1982**, *15*, 1350–1357.

(9) Terao, K.; Fujii, T.; Tsuda, M.; Kitamura, S.; Norisuye, T. *Polym. J.* **2009**, *41*, 201–207.
(10) Fujii, T.; Terao, K.; Tsuda, M.; Kitamura, S.; Norisuye, T. *Biopolymers* **2009**, *91*, 729–736.
(11) Schurig, V.; Zhu, J.; Muschalek, V. *Chromatographia* **1993**, *35*, 237–240.
(12) Kasat, R. B.; Zvinevich, Y.; Hillhouse, H. W.; Thomson, K. T.; Wang, N.-H. L.; Franses, E. I. *J. Phys. Chem. B* **2006**, *110*, 14114–14122.
(13) Kratky, O.; Porod, G. *Recl. Trav. Chim. Pays-Bas* **1949**, *68*, 1106–1122.
(14) Yamakawa, H. *Helical Wormlike Chains in Polymer Solutions*; Springer: Berlin, 1997.
(15) Yamakawa, H.; Fujii, M. *J. Chem. Phys.* **1976**, *64*, 5222–5228.
(16) Yamakawa, H. *Polym. J.* **1999**, *31*, 109–119.
(17) Yamamoto, C.; Yashima, E.; Okamoto, Y. *J. Am. Chem. Soc.* **2002**, *124*, 12583–12589.
(18) Wenslow, R. M.Jr.; Wang, T. *Anal. Chem.* **2001**, *73*, 4190–4195.
(19) Ma, S.; Shen, S.; Lee, H.; Yee, N.; Senanayake, C.; Nafie, L. A.; Grinberg, N. *Tetrahedron: Asymmetry* **2008**, *19*, 2111–2114.
(20) Kitamura, S.; Yunokawa, H.; Mitsuie, S.; Kuge, T. *Polym. J.* **1982**, *14*, 93–99.
(21) Kubota, T.; Yamamoto, C.; Okamoto, Y. *J. Am. Chem. Soc.* **2000**, *122*, 4056–4059.
(22) Berry, G. C. *J. Chem. Phys.* **1966**, *44*, 4550–4564.
(23) Norisuye, T.; Yanaki, T.; Fujita, H. *J. Polym. Sci., Polym. Phys. Ed.* **1980**, *18*, 547–558.
(24) Frisch, M. J.; Trucks, G. W.; Schlegel, H. B.; Scuseria, G. E.; Robb, M. A.; Cheeseman, J. R.; Montgomery, Jr., J. A.; Vreven, T.; Kudin, K. N.; Burant, J. C.; Millam, J. M.; Iyengar, S. S.; Tomasi, J.; Barone, V.; Mennucci, B.; Cossi, M.; Scalmani, G.; Rega, N.; Petersson, G. A.; Nakatsuji, H.; Hada, M.; Ehara, M.; Toyota, K.; Fukuda, R.; Hasegawa, J.; Ishida, M.; Nakajima, T.; Honda, Y.; Kitao, O.; Nakai, H.; Klene, M.; Li, X.; Knox, J. E.; Hratchian, H. P.; Cross, J. B.; Bakken, V.; Adamo, C.; Jaramillo, J.; Gomperts, R.; Stratmann, R. E.; Yazyev, O.; Austin, A. J.; Cammi, R.; Pomelli, C.; Ochterski, J. W.; Ayala, P. Y.; Morokuma, K.; Voth, G. A.; Salvador, P.; Dannenberg, J. J.; Zakrzewski, V. G.; Dapprich, S.; Daniels, A. D.; Strain, M. C.; Farkas, O.; Malick, D. K.; Rabuck, A. D.; Raghavachari, K.; Foresman, J. B.; Ortiz, J. V.; Cui, Q.; Baboul, A. G.; Clifford, S.; Cioslowski, J.; Stefanov, B. B.; Liu, G.; Liashenko, A.; Piskorz, P.; Komaromi, I.; Martin, R. L.; Fox, D. J.; Keith, T.; Al-Laham, M. A.; Peng, C. Y.; Nanayakkara, A.; Challacombe, M.; Gill, P. M. W.; Johnson, B.; Chen, W.; Wong, M. W.; Gonzalez, C.; Pople, J. A. *Gaussian 03, Rev. E.01*; Gaussian, Inc.: Wallingford, CT, **2004**.
(25) Andersson, M. P.; Uvdal, P. *J. Phys. Chem. A* **2005**, *109*, 2937–2941.
(26) Benoit, H.; Doty, P. *J. Phys. Chem.* **1953**, *57*, 958–963.
(27) Domb, C.; Barrett, A. J. *Polymer* **1976**, *17*, 179–184.
(28) Yamakawa, H.; Stockmayer, W. H. *J. Chem. Phys.* **1972**, *57*, 2843–2854.
(29) Shimada, J.; Yamakawa, H. *J. Chem. Phys.* **1986**, *85*, 591–599.
(30) Holtzer, A. *J. Polym. Sci.* **1955**, *17*, 432–434.
(31) Nakamura, Y.; Norisuye, T. *J. Polym. Sci., Part B: Polym. Phys.* **2004**, *42*, 1398–1407.
(32) Pedersen, J. S.; Schurtenberger, P. *J. Appl. Crystallogr.* **1996**, *29*, 646–661.
(33) Konishi, T.; Yoshizaki, T.; Saito, T.; Einaga, Y.; Yamakawa, H. *Macromolecules* **1990**, *23*, 290–297.
(34) Yamakawa, H.; Fujii, M. *Macromolecules* **1974**, *7*, 128–135.
(35) Yamakawa, H.; Yoshizaki, T. *Macromolecules* **1980**, *13*, 633–643.
(36) Barrett, A. J. *Macromolecules* **1984**, *17*, 1566–1572.
(37) Hickl, P.; Ballauff, M.; Scherf, U.; Mullen, K.; Lindner, P. *Macromolecules* **1997**, *30*, 273–279.
(38) Terao, K.; Mizuno, K.; Murashima, M.; Kita, Y.; Hongo, C.; Okuyama, K.; Norisuye, T.; Bächinger, H. P. *Macromolecules* **2008**, *41*, 7203–7210.
(39) Tsuboi, A.; Norisuye, T.; Teramoto, A. *Macromolecules* **1996**, *29*, 3597–3602.
(40) Kasabo, F.; Kanematsu, T.; Nakagawa, T.; Sato, T.; Teramoto, A. *Macromolecules* **2000**, *33*, 2748–2756.
(41) Yanagisawa, M.; Isogai, A. *Biomacromolecules* **2005**, *6*, 1258–1265.
(42) Kuse, Y.; Asahina, D.; Nishio, Y. *Biomacromolecules* **2009**, *10*, 166–173.
(43) Sutter, W.; Burchard, W. *Makromol. Chem.* **1978**, *179*, 1961–1980.
(44) Nakanishi, Y.; Norisuye, T.; Teramoto, A.; Kitamura, S. *Macromolecules* **1993**, *26*, 4220–4225.
(45) Norisuye, T. *Polym. J.* **1994**, *26*, 1303–1307.
(46) Seger, B.; Aberle, T.; Burhchard, W. *Carbohydr. Polym.* **1996**, *31*, 105–112.
(47) Significant birefringence was observed at room temperature for an ATBC900K−THF solution ($c = 0.35$ g cm^{-3}) when two polarizers were set into the cross-Nicol position. This liquid crystal had selective reflection (blue-green), indicating that its cholesteric pitch should be comparable to the wavelength of visible light.
(48) Zugenmaier, P.; Steinmeier, H. *Polymer* **1986**, *27*, 1601–1608.
(49) Takahashi, Y.; Nishikawa, S. *Macromolecules* **2003**, *36*, 8656–8661.
(50) Norisuye, T. *Prog. Polym. Sci.* **1993**, *18*, 543–584.
(51) Teramoto, A.; Fujita, H. *Adv. Polym. Sci.* **1975**, *18*, 65–149.
(52) Teramoto, A. *Prog. Polym. Sci.* **2001**, *26*, 667–720.
(53) Chisaka, S.; Norisuye, T. *J. Polym. Sci., Part B: Polym. Phys.* **2001**, *39*, 2071–2080.
(54) Mansfield, M. L. *Macromolecules* **1986**, *19*, 854–859.